AIAA JOURNAL
Vol. 43, No. 2, February 2005

Control of Edney IV Interaction by Pulsed Laser Energy Deposition

Russell G. Adelgren*
U.S. Air Force Test Pilot School, Edwards Air Force Base, California 93524
Hong Yan,† Gregory S. Elliott,‡ and Doyle D. Knight§
Rutgers University, Piscataway, New Jersey 08854-8058
Thomas J. Beutner¶
U.S. Air Force Office of Scientific Research, Arlington, Virginia 22203
and
Alexander A. Zheltovodov**
Russian Academy of Sciences, 630090, Novosibirsk, Russia

An experimental investigation was conducted to examine the effect of a pulsed Nd:YAG laser energy addition on the shock structures and surface pressure in a Mach 3.45 flow past a sphere. Two configurations were considered: 1) a sphere in a uniform freestream and 2) an Edney IV interaction generated by impingement of an oblique shock on the bow shock of the sphere. For laser energy addition upstream of the sphere in a uniform freestream, schlieren images show that the interaction of the blast wave and thermal spot cause the bow shock to move upstream while creating an expansion wave that propagates to the sphere surface. This results in a momentary 40% decrease of centerline surface pressure. The effect of the energy deposition was relatively consistent for laser energies ranging from 13 to 283 mJ/pulse. For laser energy addition upstream of an oblique shock interacting with the sphere's bow shock (Edney IV interaction), a similar thermal lensing evolution is observed, but is asymmetric due to the presence of the oblique shock. The embedded jet characteristic of the Edney IV type interaction is also perturbed as the thermal spot first interacts with the oblique shock and then the bow shock, momentarily decreasing the peak surface pressure caused by the jet by 30%.

Introduction

THE well-known Edney IV shock–shock interaction phenomena has been studied extensively along with its associated localized, intense heat transfer rates and increased surface pressures (see Refs. 1–13). An air vehicle would necessarily be designed to avoid an Edney IV interaction during normal flight. Nonetheless, an Edney IV interaction may momentarily occur due to gust response or vehicle maneuver, and therefore, either a local flow control system must be incorporated to mitigate the extreme local aerothermodynamic loads generated by the Edney IV interaction, or the vehicle aerothermal structure must be designed to withstand the momentary increased aerothermodynamic load. In this research effort, we investigate the capability of pulsed energy deposition to reduce momentarily the extreme pressure (and, therefore, possibly the heat load) associated with an Edney IV interaction.

Dynamic flow control by energy deposition has recently gained widespread interest. Knight et al.[14,15] and Zheltovodov[16] recently surveyed research efforts where aerodynamic flow control was obtained by energy deposition. They reviewed research efforts focused on the possibility of using energy deposition for drag reduction, modification of shock structures, and magnetohydrodynamic control. Researchers[17–22] have also studied the possibility of using energy deposition as a means of global flow control, that is, drag reduction of a supersonic body by means of energy deposition.

Moreover, research has been conducted on the use of energy deposition to control the sonic boom problem.[23] Others have considered it for transonic problems and for boundary-layer separation problems,[24,25] boundary-layer control,[26] and shear-layer perturbation.[27] On the other hand, energy deposition could also be used to modify localized flow problems such as the Edney IV shock–shock interaction.

The objective of this research effort is to measure the effects on the surface pressure for laser energy deposition upstream of a hemisphere at Mach 3.45 with and without an impinging shock. These experiments were performed to assess the effectiveness of using energy deposition to reduce the adverse aerodynamic loads associated with the Edney type IV shock–shock interaction upstream of a blunt body. Schlieren flow visualization was used to observe the flow with the laser perturbation and correlate with the temporal surface pressure measurements.

Background

Laser–Induced Optical Breakdown

The deposition of energy into a gas medium with a focused laser beam has been studied since the discovery in 1963 of a laser-induced spark.[28–30] Subsequent research has led to an extensive list of publications, and this research has been detailed and summarized by Raizer,[31–33] Morgan,[34] Root,[35] and Smith.[36] The overall process, described by both Root[35] and Raizer,[31–33] starts when a laser beam with sufficient power is focused down, and a sufficient radiation flux density is achieved, leading to a discharge[37,38] (somewhat similar to the electric arc discharge). The pressure and temperature of the gas in the discharge region increases significantly as the laser energy is

Received 13 December 2003; revision received 6 August 2004; accepted for publication 5 September 2004. This material is declared a work of the U.S. Government and is not subject to copyright protection in the United States. Copies of this paper may be made for personal or internal use, on condition that the copier pay the $10.00 per-copy fee to the Copyright Clearance Center, Inc., 222 Rosewood Drive, Danvers, MA 01923; include the code 0001-1452/05 $10.00 in correspondence with the CCC.

*Major, U.S. Air Force, and Director, Special Courses Division. Member AIAA.
†Research Assistant Professor, Department of Mechanical and Aerospace Engineering. Senior Member AIAA.
‡Associate Professor, Department of Mechanical and Aerospace Engineering; currently Associate Professor, Department of Aeronautical and Astronautical Engineering, University of Illinois, Urbana–Champaign, IL 61801. Member AIAA.
§Professor, Department of Mechanical and Aerospace Engineering. Associate Fellow AIAA.
¶Program Manager, Turbulence and Rotating Flows. Member AIAA.
**Head, Separated Flows Research Group. Associate Fellow AIAA.

absorbed, leading to laser-induced optical breakdown. The energy deposition into a gas by a focused laser beam can be described by five progressive steps: 1) initial release of seed electrons by multiphoton ionization, 2) rapid ionization of the gas in the focal region by the cascade release of electrons, 3) absorption and reflection of laser energy by the gaseous plasma, rapid expansion of the plasma and light-induced detonation wave formation and propagation up the focal axis, 4) propagation of the blast wave into the surrounding gas and relaxation of focal region plasma, and 5) residual vortex ring formation[39,40] due to the asymmetric formation of the plasma.

Experimental studies were conducted in Russia beginning in 1983 on the effects of laser energy deposition in supersonic flow past aerodynamic bodies. Borzov et al.[41] examined the effect of laser energy deposition on the bow shock of blunt bodies at Mach 1.5, 2.0, and 2.5, using single and pulse repetitive discharge lasers. Additional results are presented by Borzov et al.[42] including laser energy deposition in 1) quiescent air and comparison with the point explosion theory of Sedov, 2) supersonic flow with examination of the transformation of the blast wave and convection of the heated region, and 3) supersonic flow upstream of a sphere and the interaction of the heated spot with the bow shock wave. In addition, the effect of repetitive laser pulse discharges in generating a quasi-steady region of heated flow upstream of a bow shock was examined. Euler computations predicted a modification of the bow shock wave in agreement with experiments. The capability for flow control (including drag reduction) for supersonic and hypersonic aerodynamic bodies was examined.[43] Tretyakov et al.[44] performed optical flow visualization of pulsed repetitive laser energy deposition in argon at Mach 2. Tretyakov et al.[45] demonstrated experimentally the capability for drag reduction of a cone-cylinder model in supersonic flow by high-frequency CO_2 laser discharge.

Recently, Kandala and Candler[46,47] presented simulations of the laser energy deposition process for the plasma formation process (steps 1–4) for a neodymium:yttrium aluminum garnet (Nd:YAG) focused laser discharge. The Kandala and Candler model solves the conservation (mass, momentum, and energy) equations for each species along with a chemical kinetics model. The species in their model are N_2, O_2, NO, N, O, N_2^+, O_2^+, NO^+, O^+, N^+, and the electrons. Yan et al.[48] have also demonstrated a simplified gasdynamic model for the deposition into quiescent air. Dors et al.[40] have modeled the laser-induced breakdown process and observed a vortex ring formation by asymmetric plasma formation. Similarly, Svetsov et al.[49] have experimentally and numerically analyzed the postfluid motion of a laser discharge. Their findings also show a vortex formation due to an initial asymmetry. Jiang et al.[50] and Steiner et al.[51] have also numerically analyzed laser-induced blast waves.

Edney IV Shock–Shock Interaction

The present study examines the effect of pulsed energy addition upstream of the Edney IV interaction as an example of local flow control. Even though damage due to shock–shock interactions, for example, the X-15A-2 1967 Mach 6.7 test flight,[3,4] was observed before Edney's 1968 report,[5] he was the first to categorize and fully characterize the shock–shock interactions. Edney studied the effect of an oblique shock interacting with a blunt body shock and developed six categories of interactions (Fig. 1). The fourth, known as the Edney type IV interaction, is the most severe case, leading to localized regions of high surface pressure and heat transfer rates on the body. An Edney type IV interaction occurs when an oblique shock intersects a bow shock within that region where the flow immediately downstream of the bow shock would be subsonic in the absence of the interaction (Fig. 1). A supersonic jet embedded in the subsonic region behind the blunt-body bow shock develops and impinges on the blunt body (Fig. 2). This impinging, embedded supersonic jet causes high, localized heat transfer regions and high, localized surface pressures on the blunt body. These surface thermal and pressure stresses can be 10–20 times greater than stagnation conditions, thus leading to catastrophic failure of the blunt-body material for example, the X-15A-2 flight test mentioned earlier. More recently, Yamamoto et al.[52] have simulated the severity of shock impingement when space-lift booster vehicles are separated during

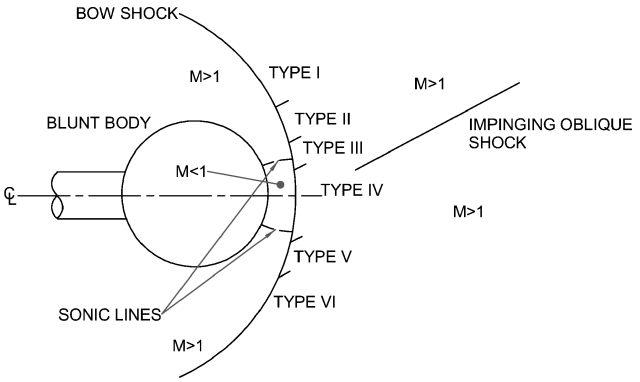

Fig. 1 Edney's shock/shock interaction classification.

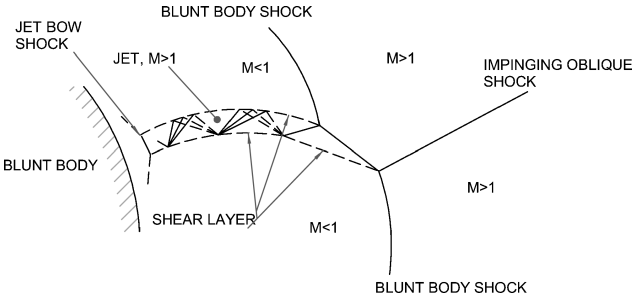

Fig. 2 Edney type-IV shock/shock interaction.

a launch environment, and Pandey[53] has simulated the structural response to the severe aerothermal loads associated with shock–shock interactions upstream of an engine cowling.

The type IV interaction has been studied both numerically and experimentally,[9,10,54–57] and the type IV shock–shock interaction has been identified as a critical hypersonic flight vehicle design issue.[8] However, no completely successful mitigation scheme has been developed to date. Borovoy et al.[11] conducted a combined computational and experimental study of type III and IV interactions at Mach 6 and 16 in air and Mach 6.6 in CO_2. The influence of the location of the impinging shock on the surface heat transfer was examined. The lower specific heat ratio in CO_2 ($\gamma = 1.3$) compared to air ($\gamma = 1.4$) had a significant influence on the flow structure and surface heat transfer in agreement with the theoretical results of Edney. Gusev and Chinilov[12] analyzed the limiting regimes of type IV interactions using an analytical method and compared the predicted surface pressure and heat transfer with experiment. The capability of modifying the peak surface pressure and heat transfer through interaction of an isentropic compression wave with the incident oblique shock wave was demonstrated. Kogan and Starodubtsev[13] performed laminar Navier–Stokes computations for a type IV interaction at Mach 6 and 16 with an assumed Gaussian heat source upstream of the interaction. The results indicate that the heat source can reduce the peak surface pressure and peak heat transfer. The total heat transfer is increased, although only a small fraction of the heat added at the source appears in the total surface heat transfer. Holden and Rodriguez,[58] Holden et al.,[58,59] and Nowak et al.[60] studied type III and IV interactions experimentally and achieved a 10% decrease in the peak heating loads with a transpiration cooling technique. Also, Modlin and Colwell[61] developed a heat exchange design to deal with the extreme heat loads generated by the type IV interaction on a hypersonic aerospace plane engine cowl. In this design, Modlin and Colwell propose using a liquid metal in a heat exchanger inside the body (an inlet cowl in this case) in addition to transpiration cooling techniques. Other researchers have further examined and characterized the shock impingement interactions. Frame and Lewis[62] developed an analytical model for type IV interaction in a calorically perfect gas without the requirement of empirical or experimental data. This analytical method is limited to two-dimensional analysis. Lind and Lewis[63,64] and Zhong[65] studied the unsteady behavior of the type IV interaction with various numerical

schemes. Hsu and Parpia[66] added complexity and studied, with numerical simulation, the effect of dual impinging oblique shocks with a bow shock interaction. Hannemann and Schnieder[67] numerically studied type III and IV interactions and developed a new classification of type IVa. Researchers have also extended the experimental analysis since Edney's classic and well-organized experimental results. Carl et al.,[68] Purpura et al.,[69] and Pot et al.[70] measured the characteristics of the interaction experimentally. Lind[71] and Berry and Nowak[72] studied the effect of body geometry on the interaction.

Experimental Apparatus

Wind Tunnel

The energy deposition tests upstream of a 25.4-mm-diam sphere with and without Edney type IV interaction were conducted in the Rutgers University Mach 3.45 supersonic wind tunnel. Table 1 lists the typical operating parameters for this facility.[73] This tunnel is a basic blowdown tunnel with an exhaust into atmospheric pressure.[74] The nozzle of the tunnel is an asymmetric one-sided nozzle that expands the flow to Mach 3.45 in the test section. The test section cross area is 15 by 15 cm, has two side windows, and has windows that can be placed in the top and bottom of the test section. Typically, these windows support optical measurement techniques and access for the laser perturbation experiments. Compressed air is supplied to the tunnel from high pressure (16.6-MPa) air storage tanks with a total volume of 8-m^3 offering run times on the order of minutes for this wind tunnel. Three four-stage air compressors supply the compressed air to these storage tanks after the moisture is removed by a regenerative air dryer.

The tunnel stagnation chamber pressure and temperature data and the atmospheric pressure for the tests are digitally recorded by a computer system. The computer system consists of a Gateway Pentium II computer with a National Instruments PCI-6031 series board, and this data acquisition system is operated with LabView software.

Flow Visualization

Schlieren images for the Mach 3.45 tunnel tests were taken in the standard Z-path arrangement[75] with 150-mm-diam concave mirrors with a focal length of 2 m. The images were recorded on a PixelVision back illuminated charge-coupled device camera with a resolution of 512 by 512 pixels. Background and flat-field images were taken to correct for uneven illumination and improve the image quality. A Stanford Research Systems pulse generator is used to control the timing delay between the pulses of the laser used for the energy deposition and the schlieren flash source. This control of the time delay allows for images to be captured for precise delays after the laser spark discharge.

A new flash source was developed. A 532-nm-wavelength Nd:YAG laser beam was focused down and discharged on a 2% thoriated tungsten rod in an argon flow for the schlieren light source. As already described, a plasma is created above the rod after seed electrons have been generated from the rod. Moreover, argon has a lower ionization threshold compared to nitrogen. For example, Mink[30] gives results showing the threshold laser power required to ionize argon at 1 atm of pressure is 70 kW, and for nitrogen at 1 atm the laser power required is 500 kW. Mink's results are for a Q-switched ruby laser and, therefore, will differ for the Nd:YAG laser used for this apparatus. In any case, the breakdown and plasma formation will be initiated more readily in argon. The half-peak pulse width for the Nd:YAG discharge in argon is 0.12 μs, and the flow transit for this time in the test section of the wind tunnel is 0.08 mm. This new spark source for the schlieren images provided much clearer and distinct flow structures due to the reduced pulse width of the strobe discharge.

Table 1 Operating parameters for the Rutgers Mach 3.45 supersonic wind tunnel

Parameter	Value
Mach number[a]	3.45
Stagnation pressure[a]	1.4 MPa
Stagnation temperature[a]	290 K
Mass flow rate	9.8 kg/s
Typical run time[a]	$\approx$ 20 s
Total run time[a]	1.8 min
Test area cross section[a]	15 cm $\times$ 15 cm
Test area length[a]	30 cm

[a]Measured quantities. [b]Calculated.

Laser for Energy Deposition

For the laser excitation experiments, a beam from a pulsed Nd:YAG 532-nm laser was focused down to create a laser-induced optical breakdown in air. The excitation beam was focused with a 250-mm focal length lens, resulting in a focal diameter of approximately less than 0.1 mm. The Nd:YAG laser was frequency doubled to a wavelength of 532 nm with a temporal pulse width of about 10 ns and a repetition rate of 10 Hz. At this pulse frequency, each perturbation can be analyzed independently because the flow transit distance between laser pulses is much larger than the tunnel test section size. The amount of energy delivered by the excitation pulse was measured using an Ophir Optronics 30A-P-SH meter. The timing of the laser was controlled with a Stanford Research Systems pulse generator, used to control the timing delay between the pulses of the laser used for the energy deposition and the schlieren imaging instrumentation.

The dimensionless parameter defining the relative energy delivered to the flow by the laser pulse is[15]

$$\varepsilon = Q_T/\rho_\infty c_p T_\infty V$$

where Q_T is the energy deposited by the laser pulse in volume V. Based on the freestream conditions (Table 2) and laser focal volume $V = 3$ mm^3, the value of ε ranged from 77 to approximately 2100 for energy pulses ranging from 13 to 283 mJ.

Sphere Model

An Edney type IV interaction is generated in the test section by the intersection of an oblique shock generated by a 15-deg wedge mounted on the test section ceiling and the bow shock of the 25.4-mm sphere mounted in the test section. The sphere model contains a pressure transducer used to measure the surface pressure (Fig. 3). The sphere model is mounted on a U joint, and the U joint in turn is mounted to a sting and splitter plate at the back of the test section (Fig. 4).

A single Endevco 8530C-100 pressure transducer is mounted inside the 25.4-mm-sphere model behind a 1.32-mm-diam port and at a depth of 1.78 mm from the front of the model's spherical surface (Fig. 3). This port was utilized to help protect the transducer and reduce the effective area of pressure sensitivity so that it could be better localized and the position measured. The fundamental frequency of the organ-pipe resonance ($a/4L$, where a is the speed of sound and L is the length of the cavity) would be expected to be

Table 2 Pressure port locations[a]

Without shock impingement			With shock impingement	
13 mJ/ pulse	127 mJ/ pulse	258 mJ/ pulse	Low position	High position
56	57	57	−57	−55
46	47	46	−46	−44
37	39	36	−31	−31
28	30	29	−16	−12
19	19	19	0	−2
11	12	10	3	4
1	1	0	10	6
−8	−10	−9	21	18
−18	−19	−19	29	29
−29	−30	−32	38	40
−42	−43	−43	51	52
−56	−55	−55	56	

[a]Port location in degrees from horizontal.

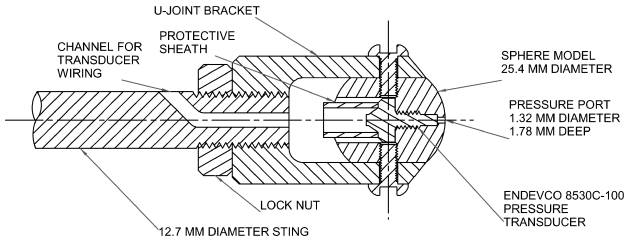

Fig. 3 Sphere surface pressure model.

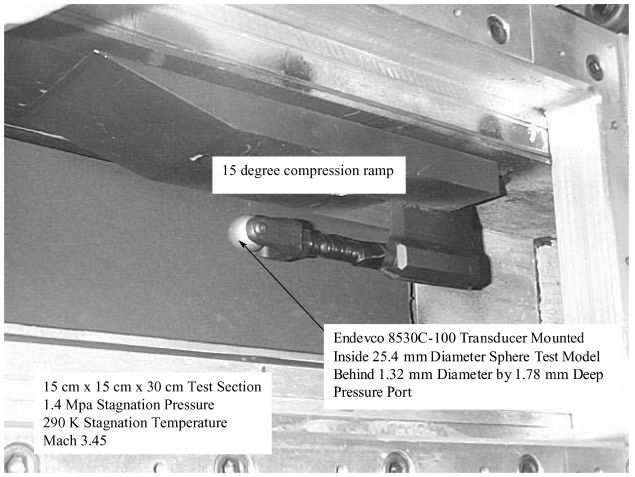

Fig. 4 Pressure model mounted in wind tunnel.

on the order of 49 kHz, but was found to be minimal in comparison to the signals measured in the results presented here and low enough in frequency so that the natural frequency of the transducer is not excited. The pressure transducer is reported by the manufacturer to have a natural frequency of 500 kHz and a flat frequency response up to 100 kHz. The rise time to which the transducer will respond linearly within $\pm 5\%$ is reported to be 2.5 μs. The uncertainty of the recorded pressure measurements is estimated to be ± 0.7 psi (4.826×10^3 Pa). The electronic leads connected to the transducer are secured to the sting and sting mount and are taken out along a channel in the sting mount through the top, rear of the test section. The signal from the transducer is conditioned by the Endevco Model 109 Piezoresistive Conditioner and filtered by an analog Krohn-Hite 3103A high- and low-pass filter set at 10 Hz and 200 kHz, respectively. The filters were set to reduce effects of low-frequency noise and high-frequency ringing from the natural frequency of the transducer. The pressure signal is recorded by a 500-MHz Hewlett–Packard digital oscilloscope data and stored in 1 μs increments to an ASCII file. The pressure data was averaged for multiple pressure traces.

The model is vertically rotated by means of the U joint to position the location of the pressure port. The uncertainty of the angle port position is ± 3 deg. Additionally, the model was mounted such that the Mach cone coming off of the wedge corners did not impact on the sphere model. This positioning of the model was done to minimize any three-dimensional effects of the Mach cone's impact on the model.

The gauges typically lasted anywhere from 1 to 30 wind-tunnel runs. The gauge diaphragm is very delicate and is susceptible to damage by high-speed particle impact. Four gauges were utilized in the test program, and the wind-tunnel nozzle area and test section were continually cleaned to eliminate as much particulate matter as possible.

Results and Discussion

Steady State

Experiments were completed for a sphere at Mach 3.45 with laser energy deposition upstream of the sphere. Surface pressure measurements were made for the cases of the sphere with and without shock impingement. The overall goal of these tests was to determine whether the laser energy deposition could be used to reduce momentarily the peak pressure loads associated with the Edney type IV shock–shock interaction. Schlieren images were made to record the interaction of the laser perturbation with the sphere and to correlate with the pressure data. Figure 5a shows the laser energy deposition locations for the tests with the sphere alone. These tests were completed as a baseline case for comparison to the shock impingement test cases. Figure 5b shows the laser energy deposition locations for the sphere with the Edney type IV shock–shock interaction. The shock standoff distances measured from the schlieren images of the sphere without shock impingement were within 3% of published results.[76]

Figure 6 shows the measured surface pressure for the Mach-3.45 sphere with the Edney type IV shock impingement, and Table 2 lists the port locations for the surface pressure measurements. The

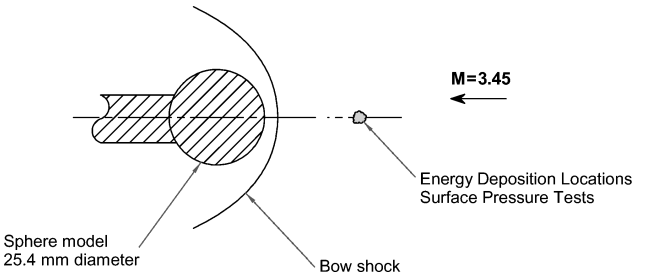

a)

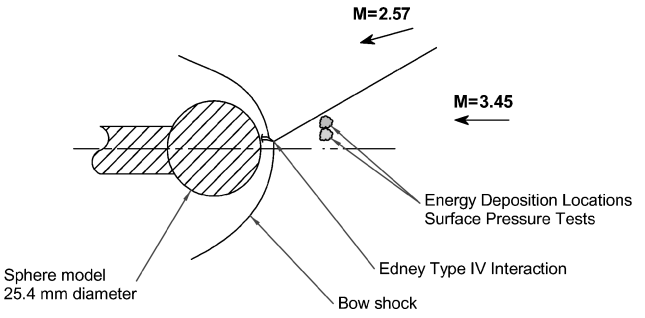

b)

Fig. 5 Laser energy deposition locations for Mach 3.45 sphere a) without shock interaction and b) with Edney type-IV shock/shock interaction.

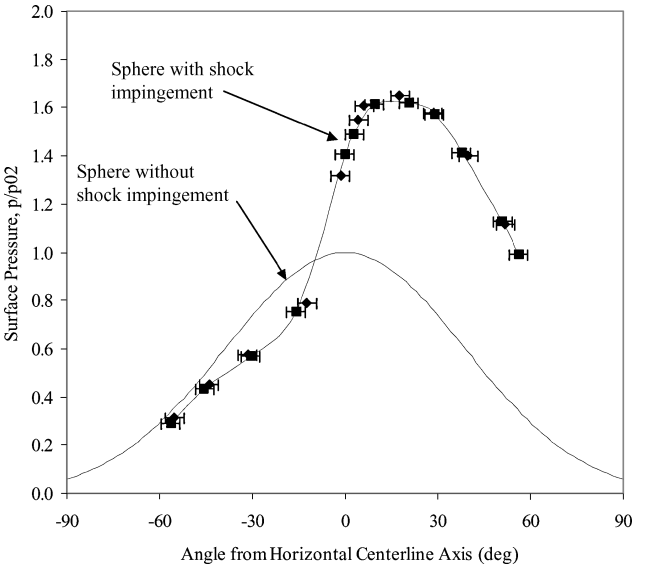

Fig. 6 Measured surface pressure for Mach 3.45 sphere with Edney type-IV shock impingement.

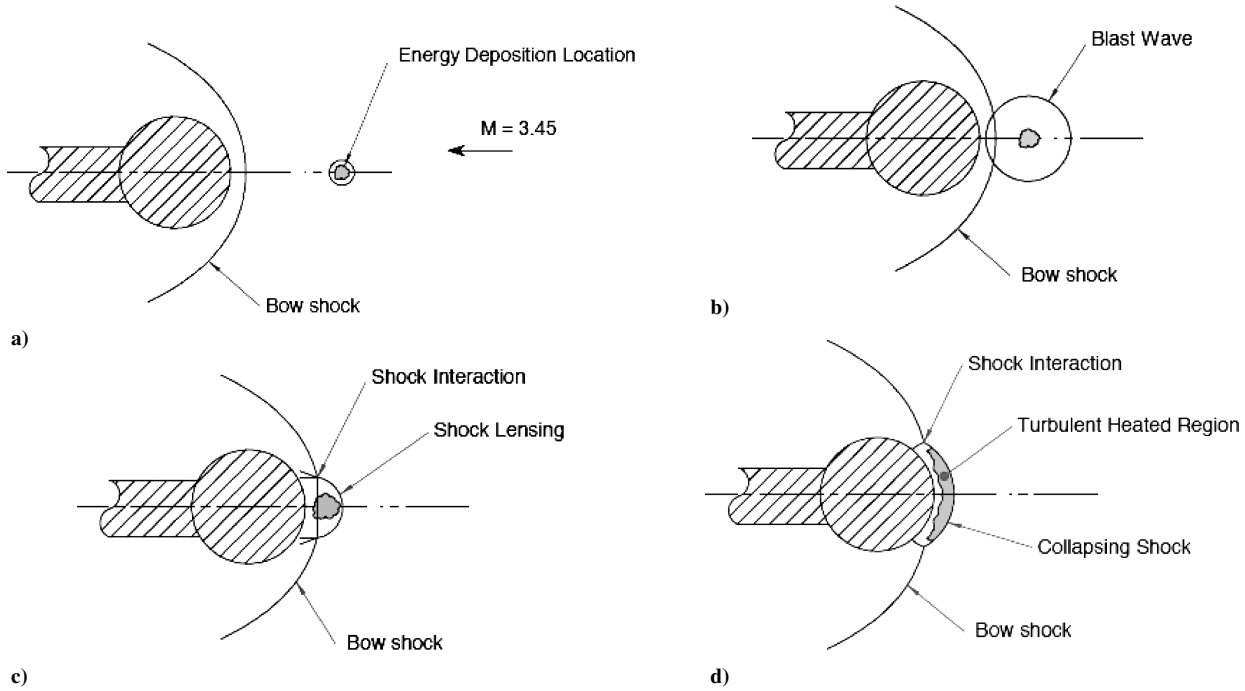

Fig. 7 Flow features for the laser energy deposition upstream of a Mach 3.45 sphere: a) initial deposition, b) blast wave effects, c) bow shock lensing due to shock thermal interface interaction, and d) thermal spot turned along the shock and bow shock collapses back to steady state.

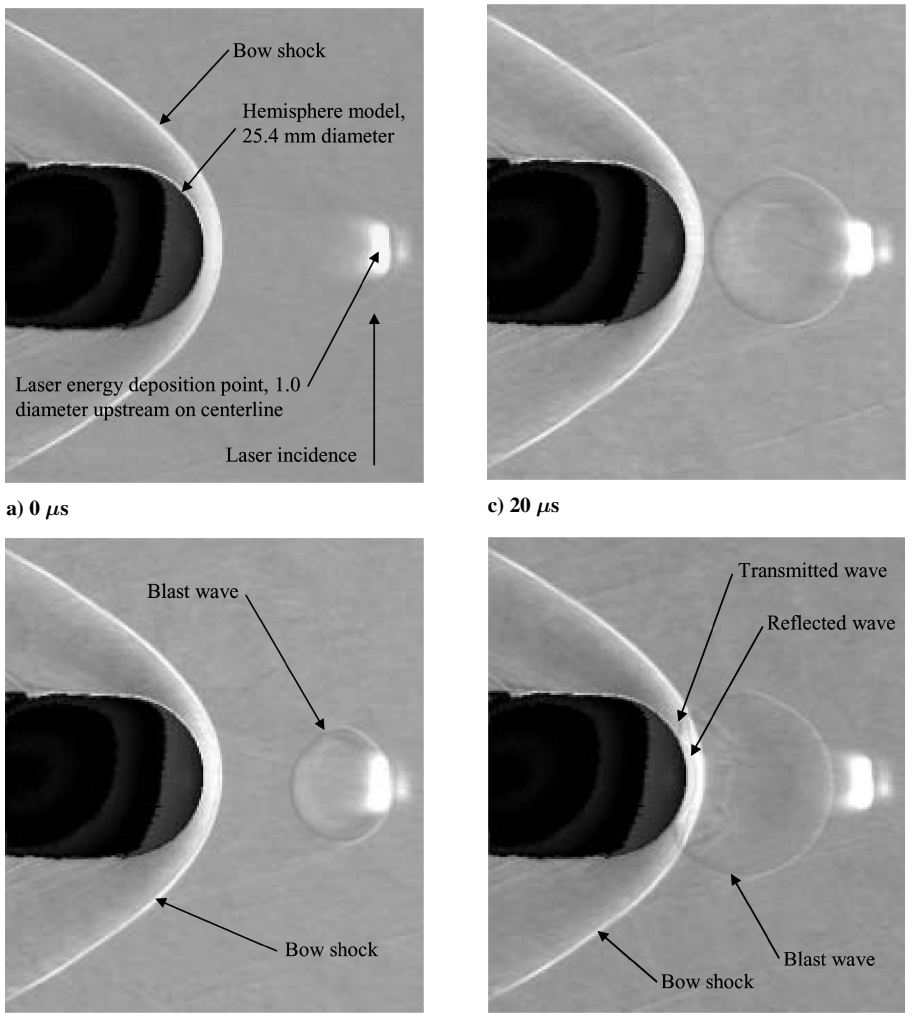

Fig. 8 Instantaneous argon/laser generated schlieren images of Mach 3.45 sphere with laser energy deposition one diameter upstream, 283 mJ/pulse, 150-mm-focal-length lens after laser deposition.

pressure has been nondimensionalized by the freestream pitot pressure. The experimental data show the characteristic rise in peak pressure due to the embedded supersonic jet of the type IV interaction. Also, Fig. 6 shows the experimental steady-state pressure distribution (without symbols for clarity) for the sphere without the shock impingement. The Euler simulation shows excellent agreement with the experimental data for the latter case.[77] The increase in surface pressure attributable to the Edney type IV shock impingement is readily seen in the comparison of the sphere-alone distribution with the measured distribution for the shock impingement case. However, this measured peak pressure is most likely lower than the actual peak pressure due to the distribution of the pressure over the pressure gauge. Because the surface of the gauge cannot be made infinitesimally small, the pressure it senses will be an average of the pressure distributed over its surface. Therefore, any numerical simulations of this experimental arrangement should take into account the finite size of the pressure port diameter and its averaging effect on the pressure sensed. D'Ambrosio[78] has demonstrated the necessity for accounting for this finite pressure sensor size when comparing experimental and numerical simulation data for the Edney type IV interaction.

The two different data symbols in Fig. 6 represent two data sets collected on two different days of wind-tunnel testing. The steady-state pressure data collected on the subsequent days of testing demonstrate the repeatability of the pressure measurements for these tests.

Another factor can be attributed to the broadening of the pressure peak associated with the shock impingement. The compression ramp used to generate the impinging oblique shock was mounted to the test section ceiling within the boundary layer. The shock generated with this ramp mounted in the boundary layer will fluctuate due to the unsteady effects associated with the turbulent boundary on the ramp.[79] The fluctuations in the oblique shock will cause the shock interaction with the bow shock location to fluctuate. This, in turn, will cause the embedded supersonic jet of the Edney IV interaction to fluctuate.

Laser Energy Deposition Upstream of Sphere

The laser energy deposition technique was applied as a perturbation upstream of the 25.4-mm sphere model in the Mach 3.45 wind tunnel. For the surface pressure measurements, the laser energy was deposited one sphere diameter upstream of the sphere surface (Fig. 5a).

As a starting point, and to give an overview of the process, Fig. 7 is a schematic of some of the unsteady flow features created by depositing the laser energy upstream of the sphere. Note that the actual interaction is three dimensional, and therefore, Fig. 7 is intended to illustrate the basic features only. In all cases, for both the sphere with and without shock impingement, the energy deposition location was upstream of the bow shock and, therefore, in the supersonic region of the flow. The pulse width of the laser is 10 ns. Thus, the energy deposited into the flow can be considered an instantaneous event.

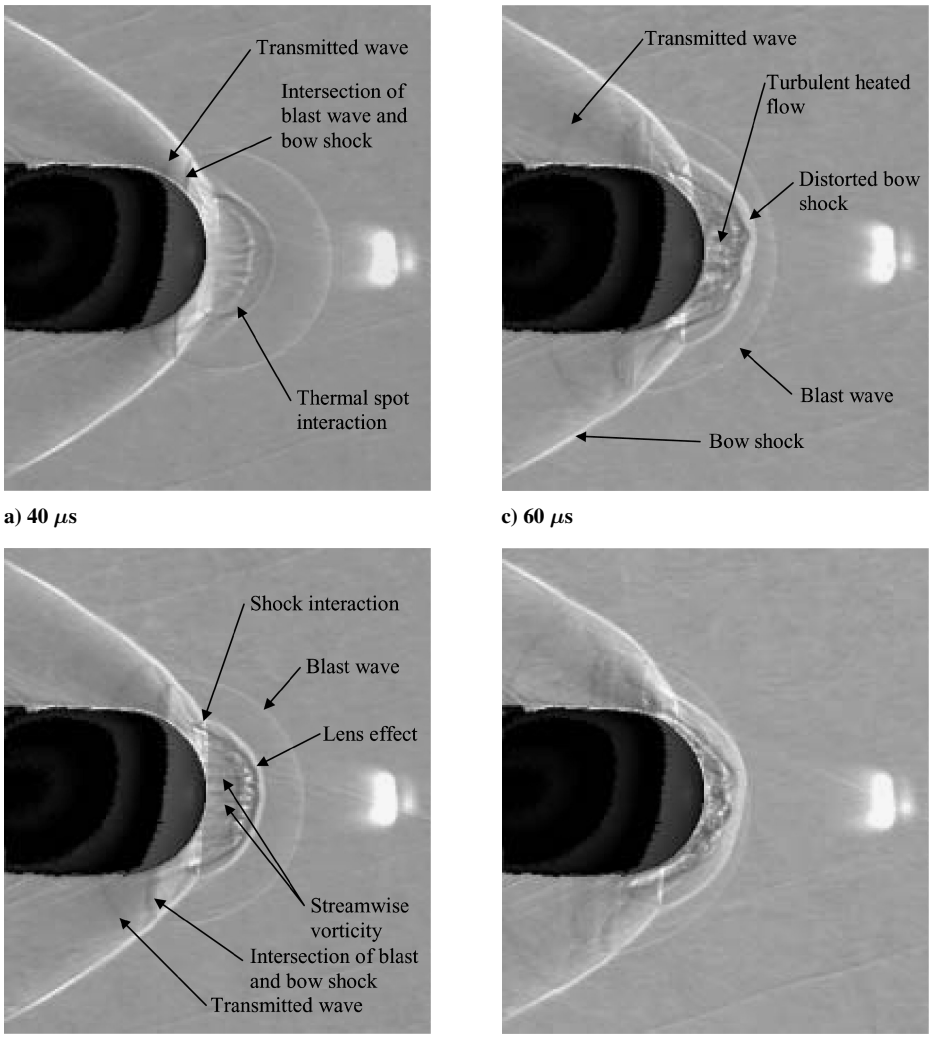

Fig. 9 Instantaneous argon/laser generated schlieren images of Mach 3.45 sphere with laser energy deposition one diameter upstream, 283 mJ/pulse, 150-mm-focal-length lens, after laser energy deposition.

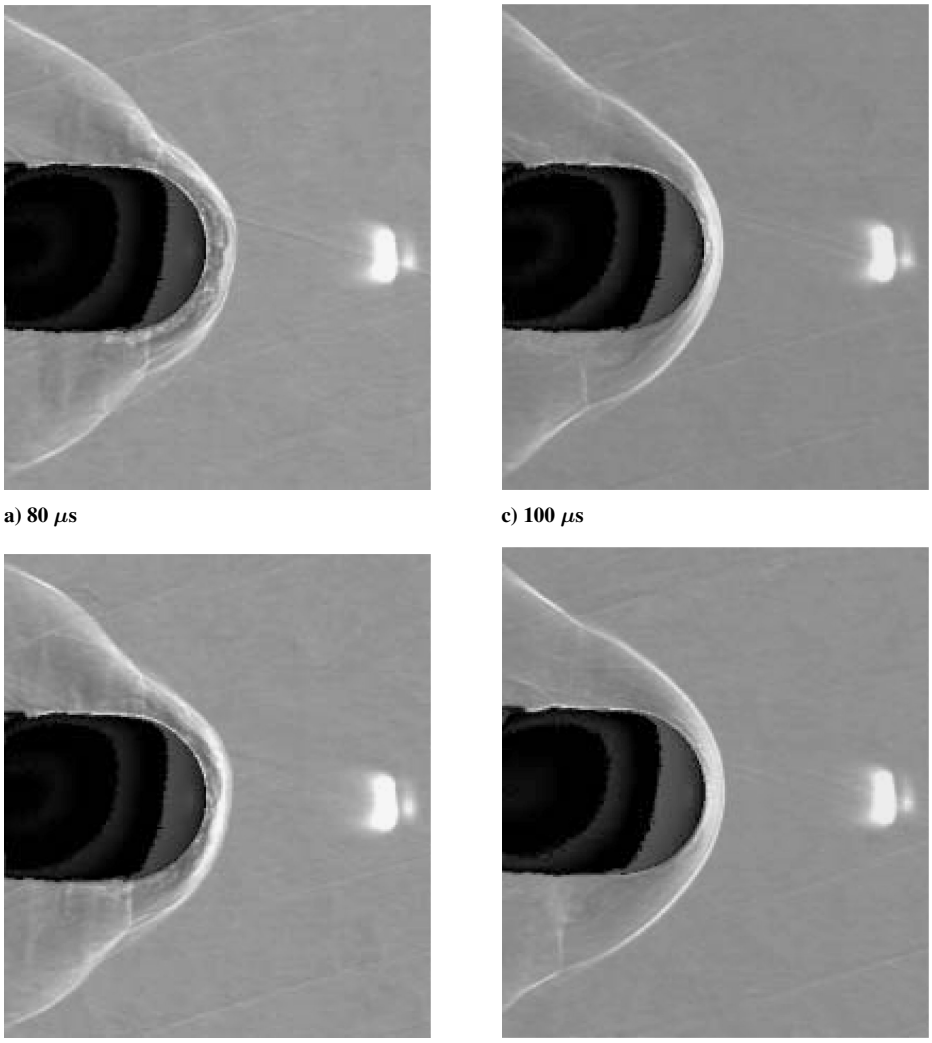

a) 80 μs **c) 100 μs**

b) 90 μs **d) 120 μs**

Fig. 10 Instantaneous argon/laser generated schlieren images of Mach 3.45 sphere with laser energy deposition one diameter upstream, 283 mJ/pulse, 150-mm-focal-length lens, after laser energy deposition.

After the laser energy has been deposited, the spot will begin to convect downstream, and a blast wave will propagate outward from the spot (Fig. 7b). The blast wave will reach the bow shock, where a weak two-shock interaction will take place (Fig. 7b). The blast wave is relatively weak compared to the bow shock. (Blast wave Mach numbers for the quiescent air tests dropped below 1.5 within 5 mm of the laser energy deposition region.[77]) However, a transmitted wave will propagate to the sphere surface. The pressure measurements detected this reflection also. (See the subsequent pressure measurement results.) The thermal spot then reaches the bow shock, where an interface/shock interaction takes place (Fig. 7c). From this interaction the bow shock lenses forward, and an expansion wave is transmitted to the sphere surface, where the pressure is reduced. The fluid within the thermal spot is turned along the shock because the stagnation pressure of the thermal spot fluid on traversing the blunt-body shock is lower than the stagnation pressure of the freestream flow that preceded it[80] (Fig. 7d).

Figure 8–10 are time sequences of instantaneous schlieren images for laser energy deposition 1.0 diameter upstream of a 25.4-mm-diam sphere in the Mach-3.45 wind tunnel. The laser for the energy deposition is repetitively fired at 10 Hz, and the flow in the test section effectively travels 64 m between laser pulses. Therefore, the schlieren images represent isolated events; however, the main features of the flow are linked in time sequence from image to image. The schlieren flash and the laser energy deposition are phase locked. The flow is from right to left in each image, and the time between the laser pulse and the schlieren spark is given beneath each image. The laser deposition location is indicated in the 0-μs-time-delay image (Fig. 8a). This spot is shown each time and is due to the flash, the bremsstrahlung effect, from the formation of the plasma region. This bright spot is visible because the shutter for the camera is open for all events, that is, the laser deposition and the schlieren flash.

The laser incidence direction for the laser energy deposition is shown in the 0-μs image (Fig. 8a). The spark is formed by focusing the 1.0-cm-diam Nd:YAG laser beam down through a 150-mm focal length lens. The optics for focusing the beam down were located below the wind-tunnel test section, and the beam was brought through the bottom test section observation window. The energy of the beam was measured at 283 mJ/pulse, and the energy deposition size is estimated at 3 ± 1 mm^3.

The blast wave is clearly visible in the schlieren image for a time delay of 10 μs between the laser pulse and the schlieren flash. At a time delay of 10 μs, the thermal spot and blast wave and the sphere/bow shock are isolated features in the flow. The knife-edge for the schlieren images is oriented vertically. The density gradients are clearly visible across the hemisphere model bow shock and the blast wave emanating from the laser energy deposition. The density gradients are in the horizontal direction for this orientation of the schlieren knife-edge.

Between 20 and 30 μs after the laser energy deposition, the blast wave for the deposition hits the bow shock of the sphere and is transmitted and then reflected off of the sphere surface. The reflected

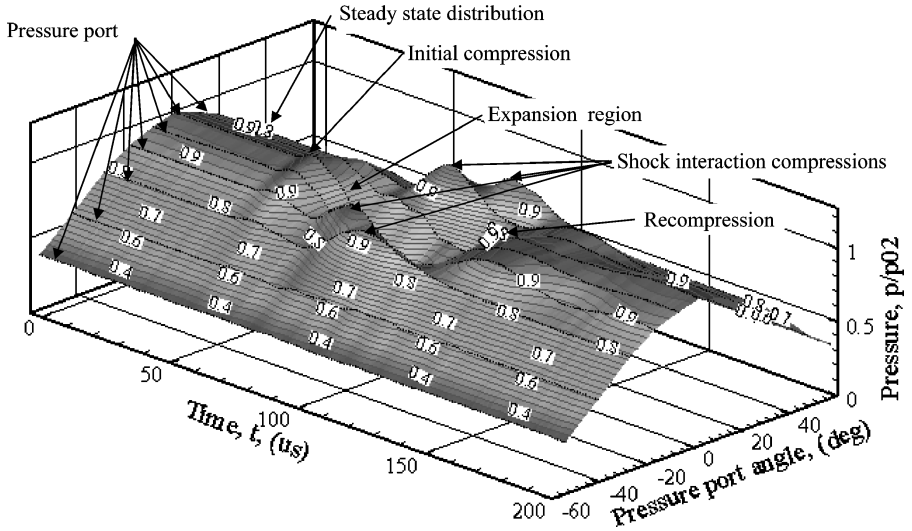

Fig. 11 Surface pressure traces for various pressure port locations on vertical symmetry plane around front of sphere with laser energy deposition (incident laser beam energy at 13 mJ/pulse) one diameter upstream and focused on model centerline.

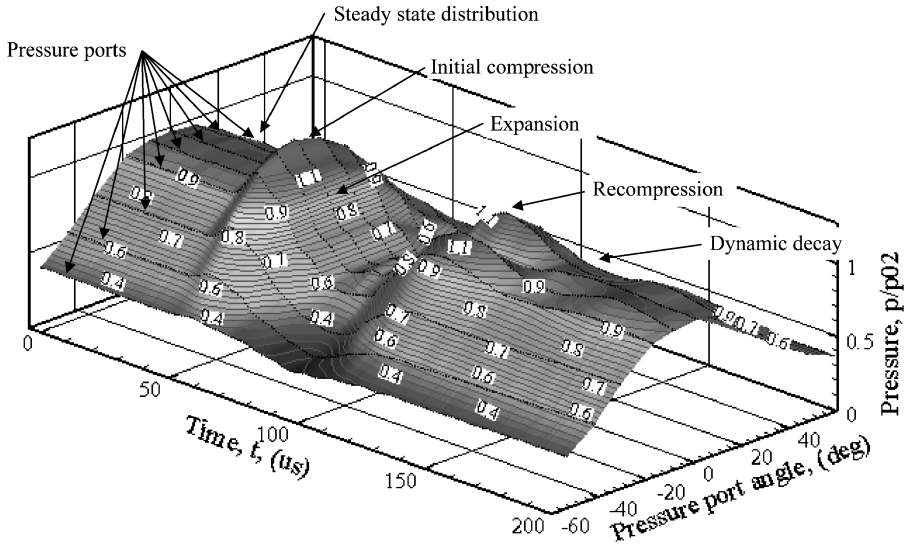

Fig. 12 Surface pressure traces for various pressure port locations on the vertical symmetry plane around front of sphere with laser energy deposition (incident laser beam energy at 127 mJ/pulse) one diameter upstream and focused on model centerline.

shock from the surface of the sphere can be seen in the 30-μs image (Fig. 8d). At 40 μs (Fig. 9a) the thermally heated region created by the laser energy deposition begins to interact with the bow shock of the hemisphere. Between 40 and 50 μs, the bow shock is distorted and blooms forward due to the decrease in local Mach number in the thermally heated region. Georgievski and Levin.[80] call this effect the lensing of the bow shock. In the 40- and 50-μs images (Figs. 9a and 9b), streamwise striations are observed. These striations represent streamwise vorticity as the three-dimensional thermal region interacts with the three-dimensional bow shock of the hemisphere.

From 60 to 70 μs (Figs. 9c and 9d), the thermal spot generated streamwise vorticity begins to breakdown to the smaller scales of turbulent flow. The distorted bow shock begins to collapse backward, and the upstream portion of the laser energy deposition blast wave moves into the bow shock. From 80 to 120 μs (Figs. 10a–10d) the bow shock collapses farther back, and the thermally heated flow convects around the sphere. Finally at 160 μs, the flow has returned to its steady-state condition.

In both of these energy deposition locations, the fluid dynamic processes occur on the order of tens of microseconds and the wave interactions on the order of microseconds. With this timescale, the

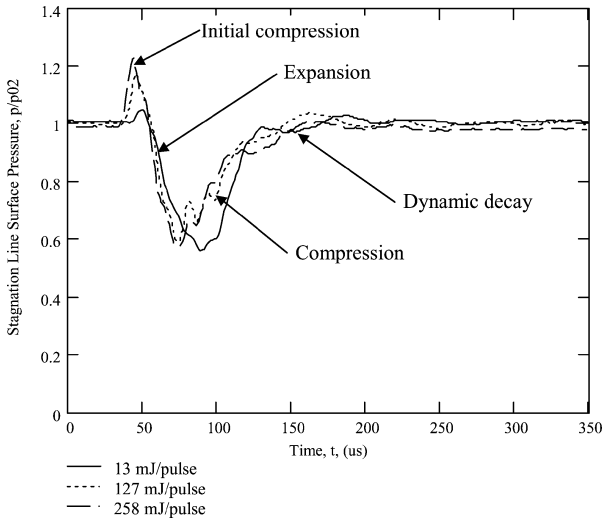

Fig. 13 Comparison of stagnation point pressure traces for sphere for three energy deposition levels 1.0 diameter upstream of the sphere.

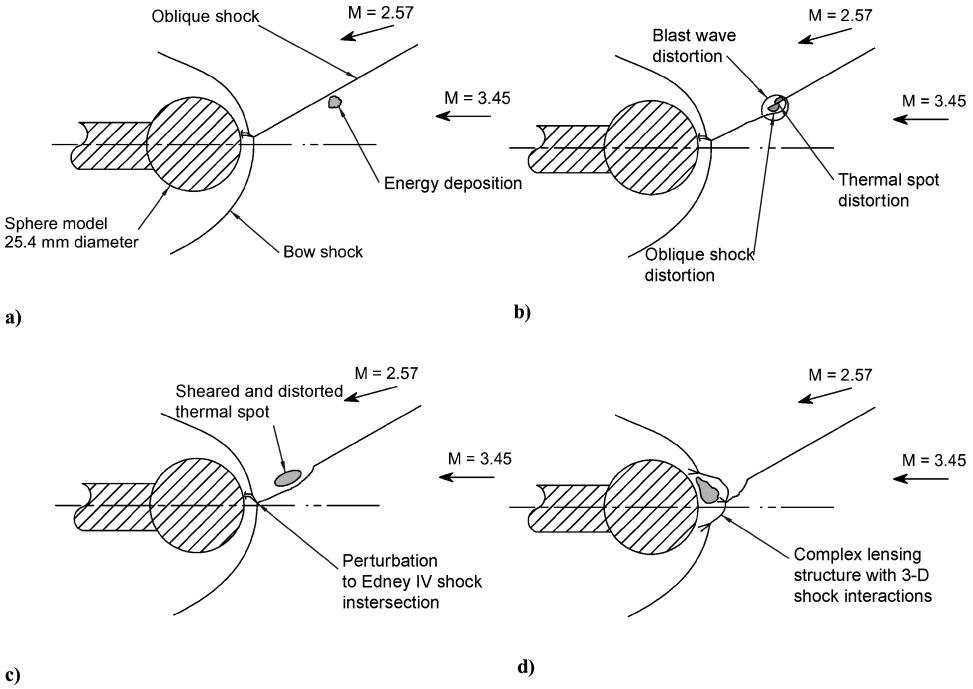

Fig. 14 Flow features associated with laser energy deposition upstream of Mach-3.45 sphere with shock impingement: a) initial deposition; b) shearing of thermal spot, oblique shock distortion, and blast wave distortion; c) perturbation to Edney IV shock–shock interaction; and d) complex bow shock lensing, thermal spot interaction with sphere, and three-dimensional shock interactions.

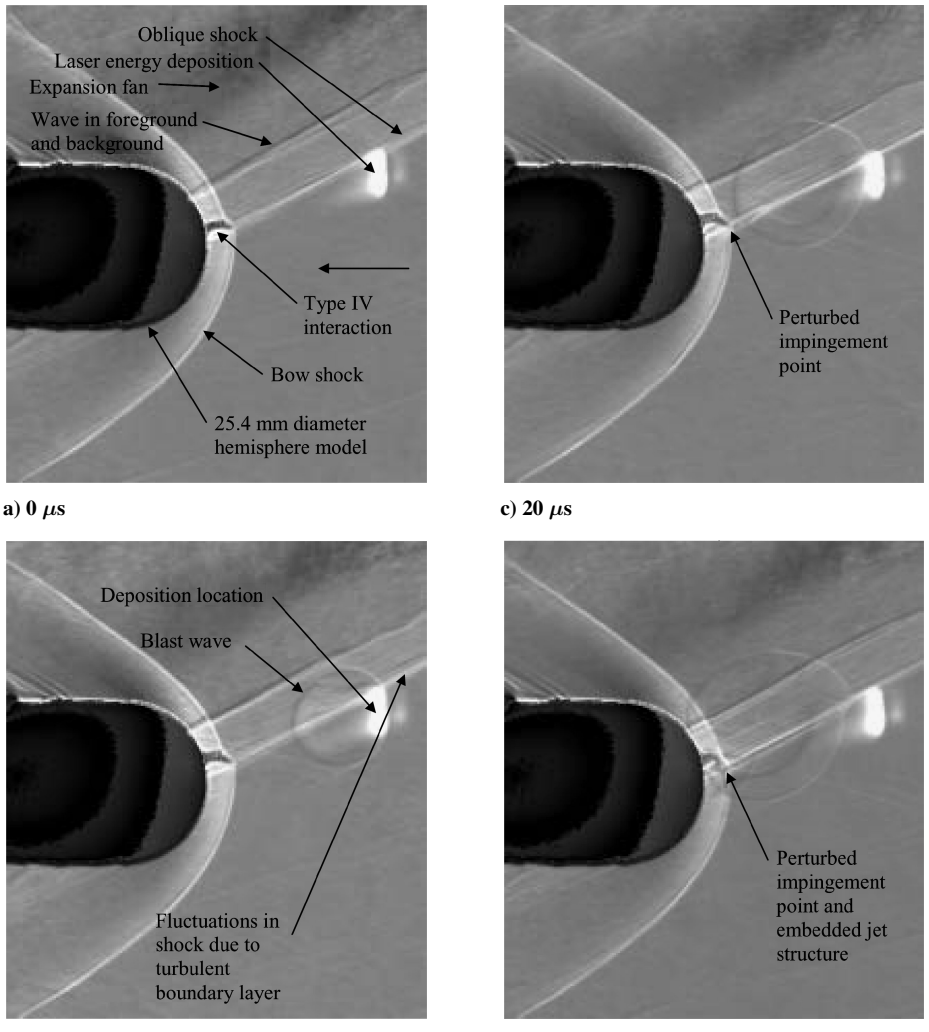

Fig. 15 Instantaneous argon/laser generated schlieren images of Mach 3.45 sphere with Edney type-IV shock impingement and with laser energy deposition 1.0 diameter upstream and 0.45 diameters above the centerline axis, 283 mJ/pulse, 150-mm-focal-length lens, after laser energy deposition.

data acquisition frequency for the surface pressure and temperature measurements were needed in the 100-kHz range.

The surface pressure was measured across the vertical symmetry plane of the sphere for laser energy deposition 1.0 diameter upstream of the front of the sphere for three energy levels: 13, 127, and 258 mJ/pulse. Figures 11 and 12 show the surface pressure from $-50 \leq \theta \leq +50$ deg as a function of time for the 13- and 127-mJ pulse energy levels. Figures 11 and 12 are constructed from a series of wind-tunnel runs with each run providing a pressure vs time trace at a fixed port angle. The pressure has been nondimensionalized with the freestream pitot pressure p_{O2}. The interaction of the thermal spot, generated by the laser discharge, with the bow shock (in the time interval of 40–90 μs) causes a blooming of the bow shock. This behavior is consistent with the simulations of Georgievski and Levin.[80] and Aleksandrov et al.[81] Note that the energy deposition affects the flow over a period on the order of 50 μs. This flow transient effect is much greater than the energy deposition whereby the excitation laser has a pulse width of 10 ns. Figure 13 shows a comparison of the centerline surface pressure traces for the three energy deposition levels. The expansion process and reduction in pressure appear to be independent of the energy level used for the deposition. However, the blast wave is stronger for the larger energy level. This effect can be seen by the larger initial compression level measured for the larger energy level and the lower compression associated with the lower energy level.

Laser Energy Deposition Upstream of Sphere with Shock Impingement

Various energy deposition locations were tested for the Mach-3.45 sphere with shock impingement (Fig. 5b). In this section, time-sequenced schlieren images are presented to assess qualitatively the effect of the laser energy perturbation on the sphere with an Edney type IV shock–shock interaction.

The main flow features are diagrammed in Fig. 14 for the laser energy deposition upstream of the Mach-3.45 sphere with the Edney type IV interaction. All of the deposition locations were upstream of the bow shock and upstream of the oblique impinging shock. The laser deposition location is shown in Fig. 14a and the laser pulse width is 10 ns. As the thermal spot encounters the oblique shock, it will shear and cause the oblique shock to distort three dimensionally upstream (Fig. 14b). The shock perturbation will transmit to the Edney IV impingement location and perturb the shock structure locally at this point (Fig. 14c). This will cause a downward motion of the embedded supersonic jet. As the thermal spot interacts with the oblique shock, it will become elongated and stretched in the streamwise direction. It will also deflect downward due to the downward velocity component behind the oblique shock. Next the thermal spot will interact with the shock structure creating a complex three-dimensional flow upstream of the sphere (Fig. 14c). The shocks on either side of the impinging shock will lens upstream due to the thermal interface and shock wave interaction. Obviously, the

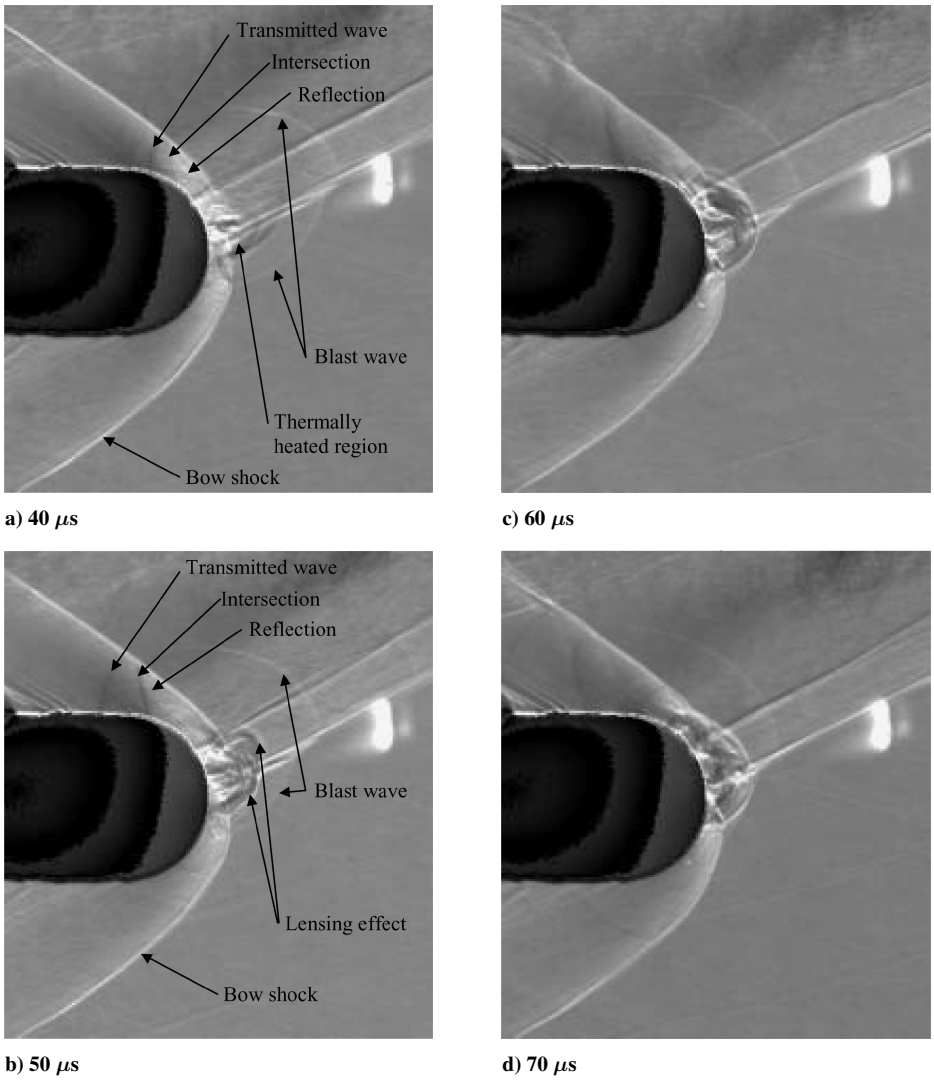

Fig. 16 Instantaneous argon/laser generated schlieren images of Mach-3.45 sphere with Edney type-IV shock impingement and with laser energy deposition 1.0 diameter upstream and 0.45 diameters above the centerline axis, 283 mJ/pulse, 150-mm-focal-length lens, after laser energy deposition.

lensing will be different on the two sides of the oblique shock. The shock will move farther upstream on the high side of the oblique shock. Complex shock interactions will form at the shock intersections (Fig. 14d). Finally, the spot will convect past the sphere, and the shock will collapse back to the steady-state Edney type IV structure. In the locations tested, the spot was low enough that it interacted with the sphere. Physical constraints limited the ability to locate the deposition location high enough so that it would perturb the impinging shock but not impact the sphere.

Figures 15–17 give instantaneous schlieren images of the Mach 3.45 sphere with Edney type IV shock–shock interaction with laser energy deposition 1.0 diameter upstream and 0.45 diameters above the centerline. The times are given below Figs. 15–17 and represent the time of the image relative to the laser energy deposition at $t = 0$ μs. As for the isolated sphere case, the blast wave and thermal spot interaction can be seen as the energy deposition interacts with the flow about the sphere.

There are two oblique shocks in Figs. 15–17. However, the upper one is due to a tunnel sidewall effect associated with the compression ramp. This upper shock is not present in the center of the test section where the sphere model is located. Filtered Rayleigh scattering images (Ref. 77) were taken in the vertical center plane to verify that this upper shock was in fact a shock in the foreground and background and not a second impinging shock on the sphere. It also appears that the impinging oblique shock extends all of the way to the surface. This apparent shock extending to the surface is a three-dimensional effect of the schlieren, and it is the oblique shock in the background and foreground of the test section, and not a shock extending down to the surface of the model.

The supersonic embedded jet set up by the Edney type IV shock–shock interaction (Fig. 2) can clearly be seen for 0 μs in Fig. 15a. The light and dark regions within the supersonic jet can be seen in the schlieren image and correspond to the compression due to the transmitted and reflected oblique shocks and the expansion regions between the shear layers of the embedded jet. These compressions, expansions, and curvature of the embedded jet are typical of the type IV interaction.[5] This supersonic embedded jet is what leads to the severe pressure and heat transfer loads to the body.

At $t = 10$ and 20 μs (Figs. 15b and 15c), the blast wave can be seen propagating outward from the laser energy deposition location. However, in contrast to the laser energy deposition upstream of the sphere, the blast wave becomes distorted as it encounters the oblique shock wave created by the compression ramp mounted to the top of the test section. At 30 μs (Fig. 15d), a distortion to the Edney type IV shock structure begins. From 50 to 80 μs (Figs. 16b–16d), the lensing of the bow shock occurs. However, in this case the lensing effect is distorted because of the difference in incident Mach numbers due to the impinging oblique shock. At 90 μs (Fig. 17b) the shock structure begins to collapse back. The flow resumes steady-state conditions by 160 μs, and the reformation of the type IV shock–shock structure.

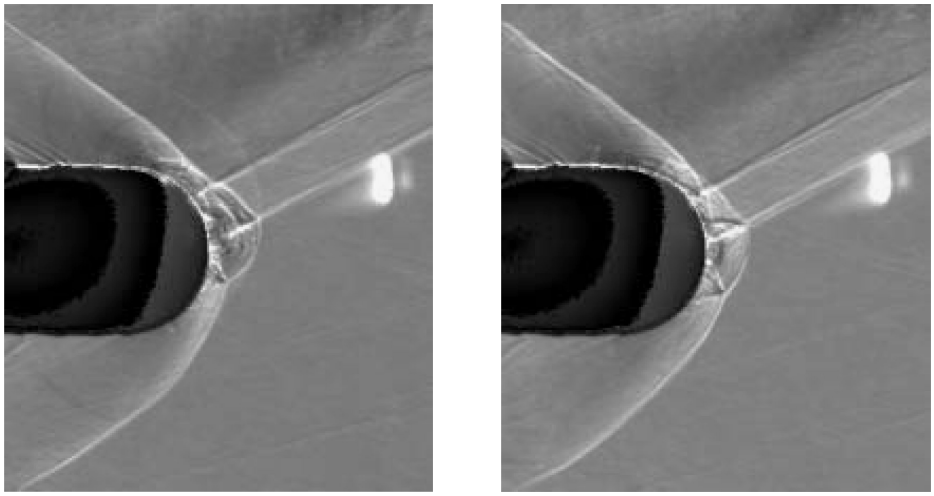

a) 80 μs

c) 100 μs

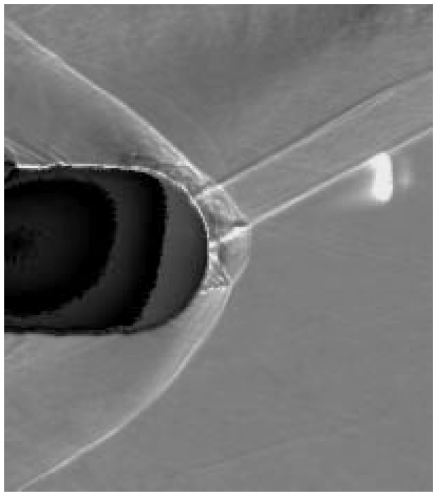

b) 90 μs

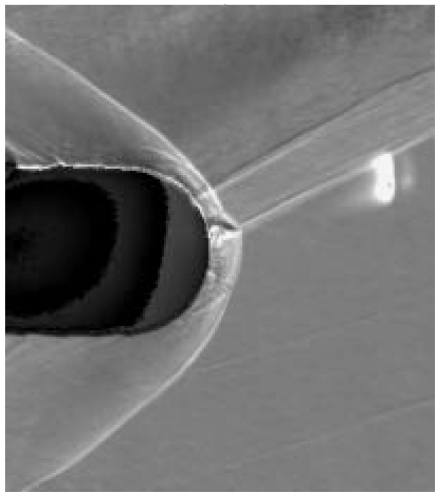

d) 110 μs

Fig. 17 Instantaneous argon/laser generated schlieren images of Mach-3.45 sphere with Edney type-IV shock impingement and with laser energy deposition 1.0 diameter upstream and 0.45 diameters above the centerline axis, 283 mJ/pulse, 150-mm-focal-length lens, after laser energy deposition.

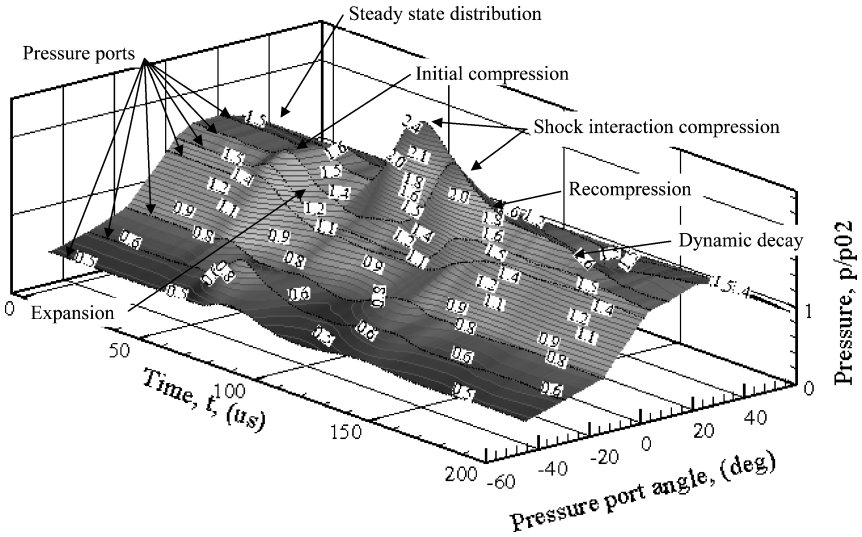

Fig. 18 Surface pressure traces on the vertical symmetry plane around front of sphere in Edney IV interaction with energy deposition 0.7 diameters upstream and 0.15 diameters above model centerline.

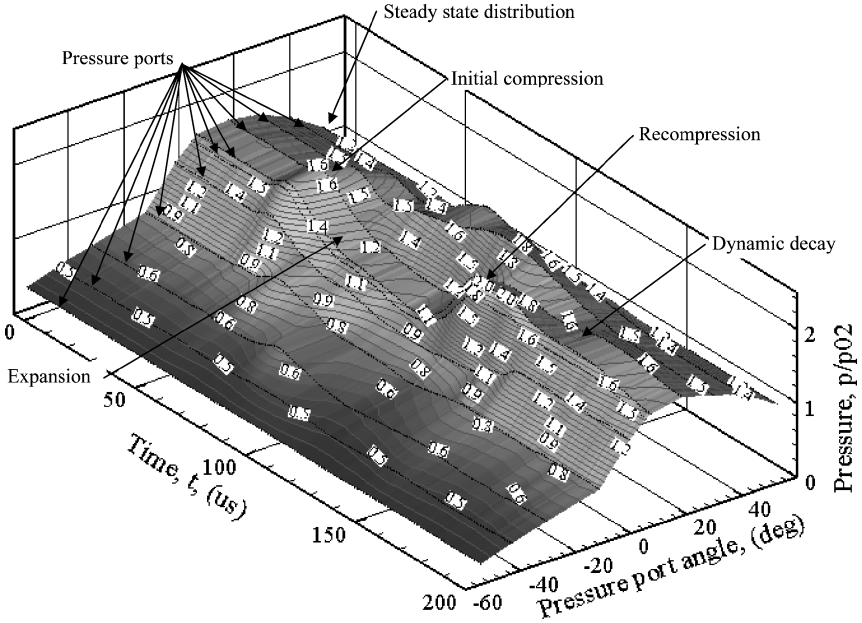

Fig. 19 Surface pressure traces on vertical symmetry plane around front of sphere in Edney IV interaction with energy deposition 0.7 diameters upstream and 0.28 diameters above model centerline.

A series of unsteady surface pressure measurements were completed for laser energy deposition upstream of the sphere model with an Edney type IV impinging shock. Table 3 lists the tunnel operating parameters for the surface pressure measurements.

Figures 18 and 19 show the surface pressure of the Mach 3.45 sphere with an Edney type IV shock interaction and with laser energy deposition upstream of the sphere. Figures 18 and 19 show the pressure as a function of time and pressure port. Both Figs. 18 and 19 show a momentary decrease in pressure similar to the thermal spot interaction with the sphere without the shock impingement. The pressure has been nondimensionalized by the freestream pitot pressure.

For the energy deposition location of 0.7 diameters upstream and 0.15 diameters above model centerline, there is an increase in the peak surface pressure 20 deg above the centerline (Fig. 18). This increase in the pressure at this location is due to a secondary-shock interaction formed by the shock lensing process and subsequent embedded jet forming and impinging on the sphere surface. This shifts the impingement location of the oblique shock and shifts the

Table 3 Tunnel operating parameters for sphere with and without shock impingement

Parameter	Sphere	Sphere with shock impingement
Mach number[a]	3.45	3.45
Reynolds number based on sphere diameter	1.71×10^6	1.86×10^6
Freestream viscosity, kg/m · s	5.32×10^{-6}	5.75×10^{-6}
Stagnation pressure, Pa	9.31×10^5	1.14×10^6
Stagnation temperature, K	263	283
Stagnation density, kg/m^3	12.3	14.0
Freestream temperature, K	77.8	83.7
Freestream pressure, Pa	1.31×10^4	1.60×10^4
Freestream density, kg/m^3	0.587	0.667
Freestream velocity, m/s	610	633
Freestream speed of sound, m/s	177	183
Pitot pressure, Pa	2.07×10^5	2.53×10^5
Pitot density, kg/m^3	2.74	3.12

[a]Measured quantities; all other quantities calculated.

location of the embedded shock. Across the bottom portion of the sphere, the pressure decreases and then increases, similar to the thermal interaction with the sphere alone.

An additional energy deposition location was tested at 0.7 diameters upstream and 0.28 diameters above the centerline (Fig. 19). However, for this case there is no significant increase in the peak pressure. The surface pressure decreases across the face of the sphere, and the peak pressure is reduced by 30% due to the thermal interaction of the laser energy deposition with the shock structure upstream of the sphere.

Conclusions

The objective of this research is evaluate the capability of pulsed Nd:YAG laser energy addition to achieve a momentary decrease in surface pressure in two configurations: 1) a sphere in a uniform freestream and 2) an Edney IV interaction generated by impingement of an oblique shock on the bow shock of the sphere. Momentary reductions in surface pressure of 40 and 30%, respectively, were achieved for the two configurations in a Mach-3.45 flow. Detailed schlieren images describe the flow phenomena associated with the interaction of the laser spot with the shock structures. These results, obtained at supersonic flow conditions, suggest that pulsed laser energy deposition should be investigated as a flow control technique for alleviating the adverse aerodynamic loads due to an Edney IV interaction encountered by a hypersonic vehicle during maneuver or gust response.

Acknowledgments

This research is supported by the U.S. Air Force Office of Scientific Research under Grant F49620-01-0368, managed by John Schmisseur, and by the U.S. Air Force Institute of Technology.

References

[1]Jenkins, D. R., "Hypersonics Before the Shuttle, A Concise History of the X-15 Research Airplane," No. 18, Monographs in Aerospace History, NASA SP 2000-4518, NASA Headquarters, Washington, DC, 2000.

[2]Burcham, F. W., and Nugent, J., "Local Flow Field Around a Pylon-Mounted Dummy Ramjet Engine on the X-15-2 Airplane for Mach Numbers 2.0 to 6.7," NASA TN D-5638, NASA Flight Research Center, Edwards AFB, CA, Feb. 1970.

[3]Watts, J. D., "Flight Experience with Shock Impingement and Interference Heating on the X-15-2 Research Airplane," NASA TM X-1669, NASA Ames Research Center, Moffett Field, CA, Oct. 1968.

[4]Watts, J. D., and Olinger, F. V., "Heat-Transfer Effects of Surface Protuberances on the X-15 Airplane," NASA TM-1566, NASA Flight Research Center, Edwards AFB, CA, May 1968.

[5]Edney, B., "Anomalous Heat Transfer and Pressure Distributions on Blunt Bodies at Hypersonic Speeds in the Presence of an Impinging Shock," Aeronautical Research Inst. of Sweden, FAA Rept. 115, Stockholm, 1968.

[6]Dana, W. H., "The X-15 Airplane-Lessons Learned," AIAA Paper 93-0309, Jan. 1993.

[7]Van Wie, D. M., White, M. E., and Corpening, G. P., "NASP Inlet Design and Testing Issues," *Johns Hopkins APL Technical Digest*, Vol. 11, No. 3 and 4, 1990, pp. 100–109.

[8]Knight, D., "RTO WG 10: Test Cases for CFD Validation of Hypersonic Flight," AIAA Paper 2002-0433, Jan. 2002.

[9]Holden, M. S., and Wadhams, T. P., "Code Validation Study of Laminar Shock/Boundary Layer and Shock/Shock Interactions in Hypersonic Flow, Part A: Experimental Measurements," AIAA Paper 2001-1031, Jan. 2001.

[10]Harvey, J. K., Holden, M. S., and Wadhams, T. P.,"Code Validation Study of Laminar Shock/Boundary Layer and Shock/Shock Interactions in Hypersonic Flow, Part B: Comparison with Navier–Stokes and DSMC Solutions," AIAA Paper 2001-1031, Jan. 2001.

[11]Borovoy, V. Y., Chinilov, A. Y., Gusev, V. N., Struminskaya, I. V., Delery, J., and Chanetz, B., "Interference Between a Cylindrical Bow Shock and a Plane Oblique Shock," *AIAA Journal*, Vol. 35, No. 11, 1997, pp. 1721–1728.

[12]Gusev, V. N., and Chinilov, A. Y., "Interference of Bow Shock Wave with Oblique Shock Wave and Isentropic Compression Wave," *Fluid Dynamics*, Vol. 38, No. 4, 2003, pp. 612–619.

[13]Kogan, M. N., and Starodubtsev, M. A., "Reduction of Peak Heat Fluxes by Supplying Heat to the Free Stream," *Fluid Dynamics*, Vol. 38, No. 1, 2003, pp. 115–125.

[14]Knight, D., Kuchinskiy, V., Kuranov, A., and Sheikin, E., "Aerodynamic Flow Control at High Speed Using Energy Deposition," *Fourth Workshop on Magneto-Plasma Aerodynamics for Aerospace Applications*, Inst. for High Temperatures, Russian Academy of Sciences, Moscow, 2002, pp. 14–30.

[15]Knight, D., Kuchinskiy, V., Kuranov, A., and Sheikin, E., "Survey of Aerodynamic Flow Control at High Speed By Energy Deposition," AIAA Paper 2003-0525, Jan. 2003.

[16]Zheltovodov, A. A., "Development of the Studies on Energy Deposition for Application to the Problems of Supersonic Aerodynamics," Inst. of Theoretical and Applied Mechanics, Preprint No. 10-2002, Novosibirsk, Russia, 2002.

[17]Chernyi, G. G., "Some Recent Results in Aerodynamic Applications of Flows with Localized Energy Addition," AIAA Paper 99-4819, Nov. 1999.

[18]Levin, V., and Terent'eva, L., "Supersonic Flow Over a Cone with Heat Release in the Neighborhood of the Apex," *Mekhanika Zhidkosti I Gaza*, Vol. 2, 1993, pp. 110–114.

[19]Myrabo, L. N., and Raizer, Y. P., "Laser-Induced Air Spike for Advanced Transatmospheric Vehicles," AIAA Paper 94-2451, June 1994.

[20]Pilyugin, N., Talipov, R., and Khlebnikov, V., "Supersonic Flow over the Bodies by the Flow with Physical–Chemical Heterogeneity," *Thermophysics of High Temperatures*, Vol. 35, No. 2, 1997, pp. 322–336.

[21]Riggins, D., Nelson, H. F., and Johnson, E., "Blunt-Body Wave Drag Reduction Using Focused Energy Deposition," *AIAA Journal*, Vol. 37, No. 4, 1999, pp. 460–467.

[22]Tretyakov, P. K., Fomin, V. M., and Yakovlev, V. I., "New Principles of Control of Aerophysical Processes—Research Development," *International Conference on the Methods of Aerophysical Research*, Inst. of Theoretical and Applied Mechanics, Novosibirsk, Russia, 1996, pp. 210–220.

[23]Miles, R., Martinelli, L., Macheret, S., Shneider, M., Girgis, I., Zaidi, S., Mansfield, D., Siclari, M., Smereczniak, P., Kashuba, R., and Vogel, P., "Suppression of Sonic Boom by Dynamic Off-Body Energy Addition and Shape Optimization," AIAA Paper 2002-0150, Jan. 2002.

[24]Schmisseur, J. D., "Receptivity of the Boundary Layer on a Mach-4 Elliptic Cone to Laser-Generated Localized Freestream Perturbations," Ph.D. Dissertation, Purdue Univ., Lafayette, IN, 1997.

[25]Adelgren, R., Elliott, G., Knight, D., Beutner, T., Ivanov, M., and Zheltovodov, A., "Laser Energy Deposition in Transverse Wall Jets and Intersecting Shocks," *Second Workshop on Thermochemical Processes in Plasma Aerodynamics*, Holding Co. Leninetz, St. Petersburg, Russia, 2001, pp. 82–98.

[26]Corke, T., Jumper, E., Post, M., Orlov, D., and McLaughlin, T., "Application of Weakly-Ionized Plasmas as Wing Flow-Control Devices," AIAA Paper 2002-0350, Jan. 2002.

[27]Adelgren, R., Elliott, G., Crawford, J., Carter, C., Grosjean, D., and Donbar, J., "Axisymmetric Jet Shear Layer Excitation Induced by Electric Arc Discharge and Focused Laser Energy Deposition," AIAA Paper 2002-0729, Jan. 2002.

[28]Damon, E. K., and Tomlinson, R. G., "Observation of Ionization of Gases by a Ruby Laser," *Applied Optics*, Vol. 2, No. 5, 1963, pp. 546–547.

[29]Maker, P. D., Terhune, R. W., and M., S. C., "Optical Third Harmonic Generation," *Quantum Electronics—Proceedings of the 3rd International Congress*, Columbia Univ. Press, New York, 1964, pp. 1559–1572.

[30]Mink, R. W., "Optical Frequency Electrical Discharges in Gases," *Journal of Applied Physics*, Vol. 35, No. 1, 1964, pp. 252–254.

[31]Raizer, Y. P., "Breakdown and Heating of Gases Under the Influence of a Laser Beam," *Soviet Physics Uspekhi*, Vol. 8, No. 5, 1966, pp. 650–673.

[32]Raizer, Y. P., *Laser-Induced Discharge Phenomena*, Consultants Bureau, New York, 1977.

[33]Raizer, Y. P., *Gas Discharge Physics*, Springer-Verlag, New York, 1997.

[34]Morgan, G. C., "Laser-Induced Breakdown of Gases," *Reports on Progress in Physics*, Vol. 38, No. 5, 1975, pp. 621–665.

[35]Root, R. G., *Laser-Induced Plasmas and Applications*, edited by L. J. Radziemski, and D. A. Cremers, Marcel Dekker, New York, 1989, pp. 69–101.

[36]Smith, D. C., "Laser Induced Gas Breakdown and Plasma Interaction," AIAA Paper 2000-0716, Jan. 2000.

[37]Meyerand, R. G., and Haught, A. F., "Gas Breakdown at Optical Frequencies," *Physical Review Letters*, Vol. 11, No. 9, 1963, pp. 401–403.

[38]Meyerand, R. G., and Haught, A. F., "Optical-Energy Absorption and High-Density Plasma Production," *Physical Review Letters*, Vol. 13, No. 1, 1964, pp. 7–9.

[39]Adelgren, R., Elliott, G., Knight, D., Zheltovodov, A., and Beutner, T., "Energy Deposition in Supersonic Flows," AIAA Paper 2001-0885, Jan. 2001.

[40]Dors, J., Parigger, C., and Lewis, J., "Fluid Dynamics Effects Following Laser-Induced Optical Breakdown," AIAA Paper 2000-0717, Jan. 2000.

[41]Borzov, V. Y., Mikhailov, V. M., Savishenko, N. P., and Yuriev, A. S., *Methods of Investigations of Aero-Thermodynamics Performances of Hypersonic Vehicles*, TsAGI, Zhukovskii Region, Russia, 1992, pp. 27, 28.

[42]Borzov, V. Y., Mikhailov, V. M., Ribka, I. V., and Savishenko, N. P., "Experimental Research of Supersonic Flow over the Obstacle at the Energy Supply into the Undisturbed Flow," *Inzhenerno-Fizichaskyi Zhurnal*, Vol. 66, No. 5, 1994, pp. 515–520.

[43]Yuriev, A. S., Borzov, V. Y., Ribka, I. V., Savishenko, N. P., and Kuranov, A. L., "Dependence of High-Speed Elements Aerodynamics on Located Heat Sources in Approaching Flow—Numerical Simulation and Wind Tunnel Tests," *Second Weakly Ionized Gases Workshop*, AIAA, Norfolk, VA, 1998, pp. 232–250.

[44]Tretyakov, P. K., Grachev, G. P., Ivanchenko, A. I., Kraniev, V. L., Ponomarenko, A. G., and Tishenko, V. N., "Stabilization of Optical Discharge in Supersonic Flow of Argon," *Dokladi Academii Nauk (DAN)*, Vol. 336, No. 4, 1994, pp. 466, 467.

[45]Tretyakov, P. K., Garanin, A. F., Grachev, G. P., Kraynev, V. L., Ponomarenko, A. G., Tishenko, V. N., and Yakovlev, V. I., "The Supersonic Flow Control over the Bodies with the Use of Power Optical Pulsating Discharge," *Dokladi Academii Nauk (DAN)*, Vol. 351, No. 3, 1996, pp. 339, 340.

[46]Kandala, R., and Candler, G. V., "Computational Modeling of Localized Laser Energy Deposition in Quiescent Air," AIAA Paper 2002-2160, May 2002.

[47]Kandala, R., and Candler, G. V., "Numerical Studies of Laser-Induced Energy Deposition for Supersonic Flow Control," AIAA Paper 2003-1052, Jan. 2003.

[48]Yan, H., Adelgren, R., Boguszko, M., Elliott, G., and Knight, D., "Laser Energy Deposition in Quiescent Air," *AIAA Journal*, Vol. 41, No. 10, 2003, pp. 1988–1995.

[49]Svetsov, V., Popova, M., Rybakov, V., Artemiev, V., and Medveduk, S., "Jet and Vortex Flow Induced by Anisotropic Blast Wave: Experiment and Computational Study," *Shock Waves*, Vol. 7, No. 6, 1997, pp. 325–334.

[50]Jiang, Z., Takayama, K., Moosad, K. P. B., Onoreda, O., and Sun, M., "Numerical and Experimental Study of a Micro-Blast Wave Generated by Pulsed-Laser Beam Focusing," *Shock Waves*, Vol. 8, No. 6, 1998, pp. 337–349.

[51]Steiner, H., Gretler, W., and Hirschler, T., "Numerical Solution for Spherical Laser-Driven Shock Waves," *Shock Waves*, Vol. 8, No. 3, 1998, pp. 139–147.

[52]Yamamoto, Y., Nagai, S., Koyama, S., Hirabayashi, N., and Hozumi, K., "CFD Analysis and Wind Tunnel Experiments of Hypersonic Shock–Shock Interaction Heating for Two Hemisphere Cylinder Problem," AIAA Paper 2002-0217, Jan. 2002.

[53]Pandey, A. K., "Thermoviscoplastic Response of Engine-Cowl Leading Edge Subjected to an Oscillating Shock–Shock Interaction," *Journal of Spacecraft*, Vol. 30, No. 6, 1993, pp. 771–773.

[54]Holden, M. S., and Kolly, J., "Measurements of Heating in Regions of Shock/Shock Interaction in Hypersonic Flow," AIAA Paper 95-0640, Jan. 1995.

[55]Holden, M. S., Kolly, J., and Martin, S., "Shock/Shock Interaction Heating in Laminar and Low-Density Hypersonic Flows," AIAA Paper 96-1866, June 1996.

[56]Weiting, A. R., and Holden, M. S., "Experimental Study of Shock Wave Interference Heating on a Cylindrical Leading Edge at Mach 6 and 8," AIAA Paper 87-1511, June 1987.

[57]Holden, M. S., Weiting, A. R., Moselle, J. R., and Glass, C., "Studies of Aerothermal Loads Generated in Regions of Shock/Shock Interaction in Hypersonic Flow," AIAA Paper 88-0477, Jan. 1988.

[58]Holden, M. S., and Rodriguez, K. M., "Studies of Shock/Shock Interaction on Smooth and Transpiration-Cooled Hemispherical Nosetips in Hypersonic Flow," NASA CR189585, April 1992.

[59]Holden, M. S., Rodriguez, K. M., and Nowak, R. J., "Studies of Shock/Shock Interaction on Smooth and Transpiration-Cooled Hemispherical Nosetips in Hypersonic Flow," AIAA Paper 91-1765, June 1991.

[60]Nowak, R. J., Holden, M. S., and Wieting, A. R., "Shock/Shock Interference on a Transpiration Cooled Hemispherical Model," AIAA Paper 90-1643, June 1990.

[61]Modlin, J. M., and Colwell, G. T., "Surface Cooling of Scramjet Engine Inlets Using Heat Pipe, Transpiration, and Film Cooling," *Journal of Thermophysics and Heat Transfer*, Vol. 6, No. 3, 1992, pp. 500–504.

[62]Frame, M. J., and Lewis, M. J., "Analytical Solution of the Type IV Shock Interaction," *Journal of Propulsion and Power*, Vol. 13, No. 5, 1997, pp. 601–609.

[63]Lind, C. A., and Lewis, M. J., "Unsteady Characteristics of a Hypersonic Type IV Shock Interaction," *Journal of Aircraft*, Vol. 32, No. 6, 1995, pp. 1286–1293.

[64]Lind, C. A., and Lewis, M. J., "Computational Analysis of the Unsteady Type IV Shock Interaction of Blunt Body Flows," *Journal of Propulsion and Power*, Vol. 12, No. 1, 1996, pp. 127–134.

[65]Zhong, X., "Application of Essentially Nonoscillatory Schemes to Unsteady Hypersonic Shock–Shock Interference Heating Problems," *AIAA Journal*, Vol. 32, No. 8, 1994, pp. 1606–1616.

[66]Hsu, K., and Parpia, I. H., "Simulation of Multiple Shock–Shock Interference Patterns on a Cylindrical Leading Edge," *AIAA Journal*, Vol. 34, No. 4, 1996, pp. 764–771.

[67]Hannemann, V., and Schnieder, M., *Shock–Shock Interaction in High Enthalpy Flow*, Wiley, New York, 1998.

[68]Carl, M., Hannemann, V., and Eitelberg, G., "Shock/Shock Interaction Experiments in the High Enthalpy Shock Tunnel Gottingen," AIAA Paper 98-0775, Jan. 1998.

[69]Purpura, C., Chanetz, B., Delery, J., and Grasso, F., "Type III and Type IV Shock/Shock Interferences: Theoretical and Experimental Aspects," Twenty-First International Symposium on Rarefied Gas Dynamics, July 1998.

[70]Pot, T., Chanetz, B., Lefebvre, M., and Bouchardy, P., "Fundamental Study of Shock/Shock Interference in Low Density Flow," Twenty-First International Symposium on Rarefied Gas Dynamics, July 1998.

[71]Lind, C. A., "Effect of Geometry on the Unsteady-Type IV Shock Interaction," *Journal of Aircraft*, Vol. 34, No. 1, 1997, pp. 64–71.

[72]Berry, S. A., and Nowak, R. J., "Fin Leading-Edge Sweep Effect on Shock-Shock Interaction at Mach 6," *Journal of Spacecraft and Rockets*, Vol. 34, No. 4, 1997, pp. 416–425.

[73]Stroehle, E. J., "The Design and Construction of a Wind Tunnel for Education and Research," M.S. Thesis, Rutgers, Piscataway, NJ, Oct. 1999.

[74]Pope, A., and Goin, K. L., *High Speed Wind Tunnel Testing*, Krieger, Malabar, FL, 1978.

[75]Goldstein, R. J., *Fluid Mechanics Measurements*, edited by R. J. Goldstein, Hemisphere, New York, 1983, pp. 377–397.

[76]Lobb, R. K., *The High Temperature Aspects of Hypersonic Flow*, Pergamon, New York, 1964, pp. 519–527.

[77]Adelgren, R., "Localized Flow Control with Energy Deposition," Ph.D. Dissertation, Dept. of Mechanical and Aerospace Engineering, Rutgers, Piscataway, NJ, Sept. 2002.

[78]D'Ambrosio, D., "Numerical Prediction of Laminar Shock/Shock Interactions in Hypersonic Flow," AIAA Paper 2002-0582, Jan. 2002.

[79]Yan, H., Knight, D., and Zheltovodov, A., "Large Eddy Simulation of Supersonic Compression Corner Using an ENO Scheme," *Third AFOSR International Conference on DNS and LES*, Greyden, 2001, pp. 381–388.

[80]Georgievski, P., and Levin, V., "Unsteady Interaction of a Sphere with Atmospheric Temperature Inhomgeneity at Supersonic Speed," *Mekhanika Zhidkosti I Gaza*, Vol. 4, 1993, pp. 174–183.

[81]Alexandrov, A., Vidyakin, N., and Lakutin, V., "On a Possible Mechanism of Interaction of a Shock Wave with the Decaying Plasma of a Laser Spark in Air," *Zhurnal Technicheskaya Phyzika*, Vol. 56, 1986, p. 771.

M. Auweter-Kurtz
Associate Editor